Nanoparticle Architectures Templated by SiO_2/Fe_2O_3 Nanocomposites

Dong Kee Yi,† Su Seong Lee,† Georgia C. Papaefthymiou,‡ and Jackie Y. Ying*,†

Institute of Bioengineering and Nanotechnology, 31 Biopolis Way, The Nanos, Singapore 138669, and Department of Physics, Villanova University, Villanova, Pennsylvania 19085

Received June 16, 2005. Revised Manuscript Received October 31, 2005

Reverse microemulsion techniques combined with templating strategies have led to the synthesis of four types of nanoparticles. First, homogeneous SiO_2-coated Fe_2O_3 (SiO_2/Fe_2O_3) nanoparticles with controlled SiO_2 shell thickness (1.8−30 nm) were synthesized by reverse microemulsion. These nanocomposite particles were used as templates for the deposition of a mesoporous silica shell. The iron oxide core in SiO_2/Fe_2O_3 could be partially and completely etched to produce rattle-type SiO_2/Fe_2O_3 nanoballs and hollow SiO_2 nanoballs, respectively. These facile synthetic methods led to the formation of different nanoparticle architectures with tailored silica shell thickness and porosity.

Introduction

Magnetic nanoparticles have broad applications such as data storage, bearings, lubricants, wave absorbers, magnetic resonance contrast-enhancing media, therapeutic agent in cancer treatment (e.g., hyperthermia), drug delivery, cell separation, and protein immobilization.[1] The superparamagnetic properties of these nanoparticles are of great interest for biomedical applications. However, the bare magnetic nanoparticles need to be coated with a suitable material that is biocompatible, nontoxic, and water soluble.

Polystyrene coating on iron oxide nanoparticles has been proposed using emulsion polymerization[2] and atom transfer radical polymerization.[3] Hydrophobic materials in the blood can be attacked by the immune system and removed from the body. Therefore, polystyrene-coated iron oxide systems are not suitable for in vivo applications. In contrast, SiO_2-coated magnetic nanoparticles are hydrophilic and stable against biodegradation. Furthermore, the ease of silica surface modification[4] would allow for biolabeling, drug targeting, and delivery. Stöber[5] and sol−gel processes are the prevailing methods used for coating magnetic nanoparticles with silica.[6] Aerosol pyrolysis has also been used for silica coating, but the particles produced are hollow silica spheres with magnetic shells.[7] Microemulsion has been used to prepare silica-coated magnetic nanoparticles.[6d−f] However, synthesis of uniform and controlled silica shell thickness on the nanometer scale remains challenging. Well-controlled particle size and morphology would be important for the application of SiO_2-coated magnetic nanoparticles in biomedical applications, such as magnetic resonance imaging, magnetorelaxometry, magnetic cell separation, and drug delivery. By introducing mesoporous silica[8] coating on dense SiO_2-coated magnetic nanoparticles, and by creating rattle-type silica balls with magnetic nanoparticles, applications in catalysis, chemical sensing and separations may be explored. These systems have not been reported, although Au nanoparticles with mesoporous silica shells[9a] and rattle-type silica balls with Cu cores have been examined.[9b]

* Corresponding author. E-mail: jyying@ibn.a-star.edu.sg.
† Institute of Bioengineering and Nanotechnology.
‡ Villanova University.

(1) (a) Ross, C. *Annu. Rev. Mater. Res.* **2001**, *31*, 203. (b) Hafeli, U.; Schutt, W.; Teller, J.; Zborowski, M. *Scientific and Clinical Applications of Magnetic Carriers*; Plenum Press: New York, 1998. (c) Meldrum, F. C.; Heywood, B. R.; Mann, S. *Science* **1992**, *257*, 522. (d) Dyal, A.; Loos, K.; Noto, M.; Chang, S. W.; Spagnoli, C.; Shafi, K. V. P. M.; Ulman, A.; Cowman, M.; Gross, R. J. *J. Am. Chem. Soc.* **2003**, *125*, 1684. (e) Fukushima, T.; Sekizawa, K.; Jin, Y.; Yamaya, M.; Sasaki, H.; Takishima, T. *Am. J. Physiol.* **1993**, *265*, L67. (f) Babes, L.; Denizot, B.; Tanguy, G.; Le Jeune, J. J.; Jallet, P. *J. Colloid Interface Sci.* **1999**, *212*, 474. (g) Tanaka, T.; Matsunaga, T. *Anal. Chem.* **2000**, *72*, 3518. (h) Matsunaga, T.; Kawasaki, M.; Yu, X.; Tsujimura, N.; Nakamura, N. *Anal. Chem.* **1996**, *68*, 3551. (i) Harisinghani, M. G.; Barentsz, J.; Hahn, P. F.; Deserno, W. M.; Tabatabaei, S.; van de Kaa, C. H.; de la Rosette, J.; Weissleder, R. *N. Engl. J. Med.* **2003**, *348*, 2491. (j) Levy, L.; Sahoo, Y.; Kim, K. S.; Bergey, E. J.; Prasard, P. N. *Chem. Mater.* **2002**, *14*, 3715. (k) Euliss, L. E.; Grancharov, S. G.; O'Brien, S.; Deming, T. J.; Stucky, G. D.; Murray, C. B.; Held, G. A. *Nano Lett.* **2003**, *3*, 1489. (l) Huber, D. L. *Small* **2005**, *1*, 482.

(2) Xu, X.; Friedman, G.; Humfeld, K.; Majetich, S.; Asher, S. *Adv. Mater.* **2001**, *13*, 1681.

(3) Wang, Y.; Teng, X.; Wang, J.-S.; Yang, H. *Nano Lett.* **2003**, *3*, 789.

(4) Ulman, A. *Chem. Rev.* **1996**, *96*, 1533.

(5) Stöber, W.; Fink, A.; Bohn, E. J. *J. Colloid. Interface Sci.* **1968**, *26*, 62.

(6) (a) Phillipse, A. P.; Bruggen, M. P. B.; Pathmamanoharan, C. *Langmuir* **1994**, *10*, 92. (b) Kobayashi, Y.; Horie, M.; Konno, M.; Rodriguez-González, B.; Liz-Marzan, L. M. *J. Phys. Chem. B* **2003**, *107*, 7420. (c) Lu, Y.; Yin, Y.; Mayers, B. T.; Xia, Y. *Nano Lett.* **2002**, *2*, 183. (d) Santra, S.; Tapec, R.; Theodoropoulou, N.; Dobson, J.; Hebrad, A.; Tan, W. *Langmuir* **2001**, *17*, 2900. (e) Tago, T.; Hatsuta, T.; Miyajima, K.; Kishida, M.; Tashiro, S.; Wakabayashi, K. *J. Am. Ceram. Soc.* **2002**, *85*, 2188. (f) Vestal, C. R.; Zhang, Z. J. *Nano Lett.* **2003**, *3*, 1739.

(7) Tartaj, P.; González-Carreño, T.; Serna, C. J. *Adv. Mater.* **2001**, *13*, 1620.

(8) (a) Huo, Q.; Margolese, D. I.; Ciesla, U.; Feng, P.; Gier, T. E.; Sieger, P.; Leon, R.; Petroff, P. M.; Schüth, F.; Stucky, G. D. *Nature* **1994**, *368*, 317. (b) Ying, J. Y.; Mehnert, C. P.; Wong, M. S. *Angew. Chem. Int. Ed.* **1999**, *38*, 56. (c) Ying, J. Y. *Sci. Spectra* **1999**, *18*, 56. (d) Soler-Illia, G. J. A. A.; Sanchez, C.; Lebeau, B.; Patarin, J. *Chem. Rev.* **2002**, *102*, 4093. (e) Stein, A. *Adv. Mater.* **2003**, *15*, 763. (f) Taguchi, A.; Schüth, F. *Microporous Mesoporous Mater.* **2005**, *77*, 1.

(9) (a) Kim, J. Y.; Yoon, S. B.; Yu, J. S. *Chem. Commun.* **2003**, 790. (b) Hah, H. J.; Um, J. I.; Han, S. H.; Koo, S. M. *Chem. Commun.* **2004**, 1012.

10.1021/cm0512979 CCC: $33.50
Published on Web 01/14/2006

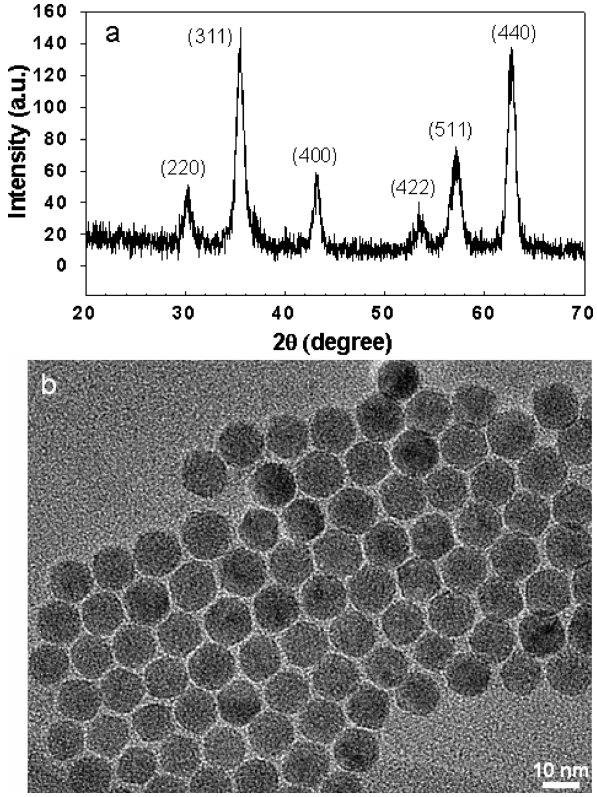

Figure 1. (a) X-ray diffraction (XRD) pattern and (b) transmission electron microscopy (TEM) images of γ-Fe_2O_3 nanocrystals.

Experimental Section

In this work, SiO_2/Fe_2O_3 nanoparticles were used as a platform for deriving other nanoparticle architectures. Uniform SiO_2/Fe_2O_3 nanoparticles were prepared using monodispersed γ-Fe_2O_3 nanocrystals (average diameter ~12.5 nm) (see Figure 1), which had been synthesized by the thermal decomposition of iron pentacarbonyl precursor in the presence of an oleic acid stabilizer and octyl ether.[10] SiO_2 coating on the γ-Fe_2O_3 nanoparticles was performed through the formation of water-in-cyclohexane reverse microemulsion[11] (see Scheme 1). Specifically, for a 10 nm thick SiO_2 shell, polyoxyethylene(5)nonylphenyl ether (0.56 mmol, Igepal CO-520, containing 50 mol % hydrophilic group) was dispersed in cyclohexane (4.2 mL) by sonication. Then, 300 μL of Fe_2O_3 solution (0.8 mg/mL of cyclohexane) was added. The resulting mixture was vortexed, and ammonium hydroxide (29.4%, 35 μL) was added to form a transparent, brown solution of reverse microemulsion. Next, tetraethyl orthosilicate (20 μL, TEOS) was added, and the reaction was continued for 16 h at room temperature. When methanol was added into the reaction solution, SiO_2/Fe_2O_3 nanoparticles were precipitated. They were collected by a magnet, washed with methanol, and redispersed in ethanol.

Cytotoxicity of the SiO_2/Fe_2O_3 nanoparticles was measured using two different cell lines, HepG2 and NIH3T3. Cell viability was measured using 3-(4,5-dimethylthiazol-2-yl)-2,5-diphenyltetrazolium bromide (MTT) assay on day 1, 2, and 3 over nanoparticle doses of 10−100 μg/mL.

Mesoporous silica-coated SiO_2/Fe_2O_3 ($MS/SiO_2/Fe_2O_3$) nanocomposite particles were prepared by stirring TEOS and octadecyltrimethoxysilane (C18TMS) (at a molar ratio of 1:4.7) in a mixture of ethanol (22 mL) and aqueous 15% NH_4OH solution (2 mL) with SiO_2/Fe_2O_3 nanoparticles at room temperature for 6 h. The product was collected by a magnet, washed with ethanol, and calcined at 823 K in air for 7 h to remove the C18TMS porogen (ramp = 1 K/min). To control the thickness of the mesoporous silica layer, the volume of TEOS and C18TMS mixture was varied from 100 to 300 μL.

Hollow SiO_2 balls and rattle-type SiO_2/Fe_2O_3 nanoballs were prepared by etching SiO_2/Fe_2O_3 nanoparticles with 20% HCl. They were collected by centrifuging at 7000 rpm for 15 min and were washed with deionized water and ethanol to remove the yellowish $FeCl_3$.

Results and Discussion

The SiO_2 shell thickness in the SiO_2/Fe_2O_3 nanoparticles could be tuned by controlling the synthesis and processing parameters. Figure 2 shows that the shell thickness increased with increasing TEOS content and aging time and decreasing Fe_2O_3 solution volume and surfactant content. The shell thickness was tunable from ~1.8 to ~30 nm. Figure 2c shows that when the surfactant content was increased beyond 0.61 mmol, no change in SiO_2 shell thickness was noted. In this special case, some core-free silica nanoparticles were observed, most likely because some of the excess surfactant formed micelles that did not contain any Fe_2O_3 nanoparticles.

Figure 3a inset illustrates a high-resolution transmission electron microscopy (HRTEM) image of γ-Fe_2O_3 nanocrystals with thin silica shells of ~1.8 nm thickness (noted by an arrow). Figure 3b illustrates SiO_2/Fe_2O_3 nanoparticles with a shell thickness of ~4 nm. The asymmetrically coated silica layers observed along the edges of the γ-Fe_2O_3 nanocrystals (noted by arrows) suggested a silica nucleation and coating process directed by γ-Fe_2O_3 nanocrystals. Similar phenomenon (noted by arrows) was noted to a lesser extent for SiO_2/Fe_2O_3 nanoparticles with thicker shells of 9 nm (Figure 3c). For nanoparticles with 25 nm thick shells (Figure 3d), symmetrical coating of SiO_2 was observed around each γ-Fe_2O_3 core, and uniform particle size and morphology were achieved.

Cytotoxicity of the SiO_2/Fe_2O_3 nanoparticles with ~25 nm thick shells was studied using two different cell lines, HepG2 and NIH3T3. The inhibitory activities of SiO_2/Fe_2O_3 nanoparticles were dependent on particle dose and period of exposure. The strongest inhibitory activity was observed on day 3 with a particle dose of 100 μg/mL. In all cases, the inhibitory concentration 50 (IC_{50}) was larger than 100 μg/mL. Such IC_{50} value was substantially higher than that of nanoparticles such as CdSe ($IC_{50} < 62.5$ μg/mL).[12] Details of the percentage of viable cells with respect to the control for a given cell type are available in the Supporting Information (SI).

Kaiser[13] was the first to report the synthesis of porous silica beads using TEOS condensation and *n*-alkyltrialkoxysilane as a porogenic material in a mixture of ethanol and aqueous NH_4OH. This method was further developed to coat solid SiO_2 particles[14] and SiO_2/Au nanoparticles.[15] While there has

(10) Hyeon, T.; Lee, S. S.; Park, J.; Chung, Y.; Na, H. B. *J. Am. Chem. Soc.* **2001**, *123*, 128.
(11) (a) Yi, D. K.; Selvan, S. T.; Lee, S. S.; Papaefthymiou, G. C.; Kundaliya, D.; Ying, J. Y. *J. Am. Chem. Soc.* **2005**, *127*, 4991. (b) Selvan, S. T.; Tan, T. T.; Ying, J. Y. *Adv. Mater.* **2005**, *17*, 1620.
(12) Derfus, A. M.; Chan, W. C. W.; Bhatia, S. N. *Nano Lett.* **2004**, *4*, 11.
(13) Kaiser, C. Ph.D. Thesis, Gutenberg Universität, Mainz, Germany, 1996.

Scheme 1. Schematic of the Synthesis of SiO_2/Fe_2O_3 Nanoparticles by Reverse Microemulsion[a]

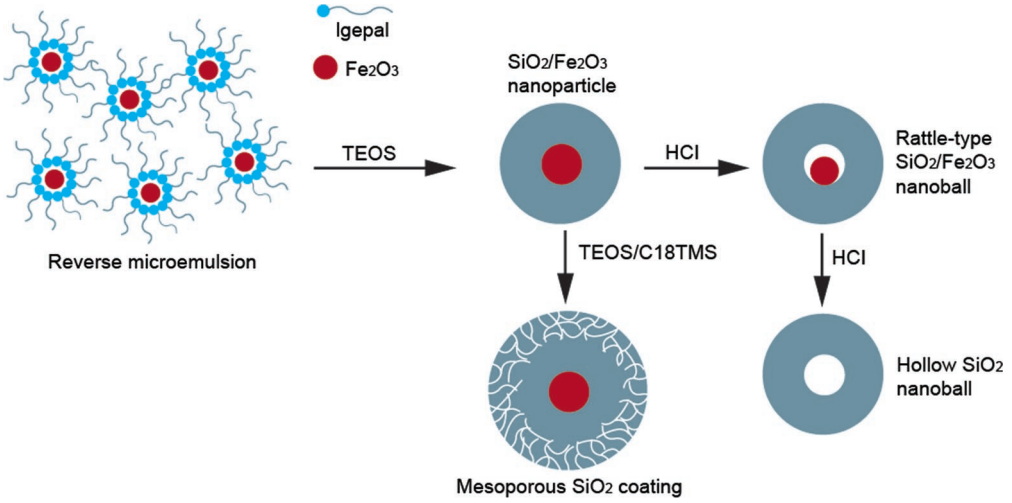

[a] These nanoparticles were then used to derive mesoporous silica-coated SiO_2/Fe_2O_3 nanoparticles, rattle-type SiO_2/Fe_2O_3 nanoballs, and hollow SiO_2 nanoballs.

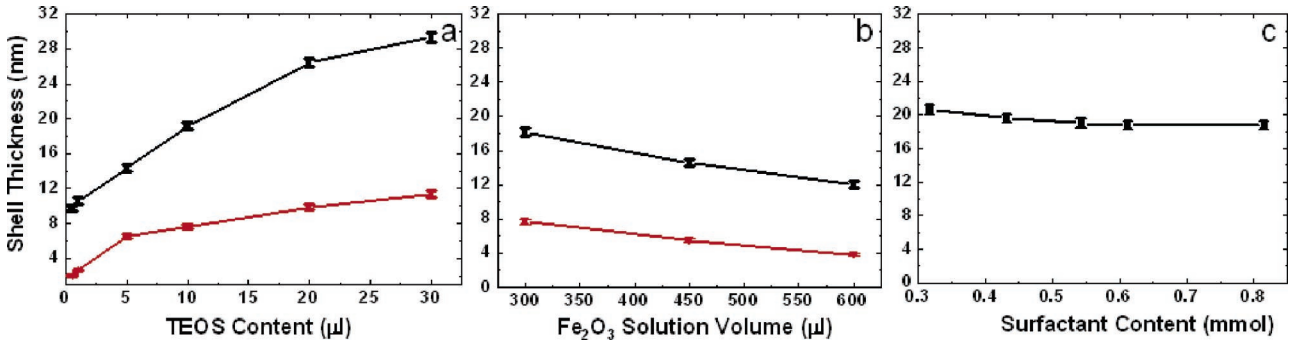

Figure 2. Effect of (a) TEOS content, (b) Fe_2O_3 solution volume, and (c) Igepal surfactant content on the SiO_2 shell thickness of SiO_2/Fe_2O_3 nanoparticles. Fixed Fe_2O_3 solution volume (300 μL) and surfactant content (0.56 mmol) were used in (a). Fixed TEOS content (10 μL) and surfactant content (0.56 mmol) were used in (b), whereby Fe_2O_3 was solubilized in cyclohexane (0.8 mg/mL of cyclohexane). In (a) and (b), the samples were aged for 16 h (red) or 240 h (black). Fixed TEOS content (30 μL), Fe_2O_3 solution volume (400 μL), and aging time (50 h) were used in (c).

been a report of magnetic nanoparticles deposited within mesoporous matrices,[16] $MS/SiO_2/Fe_2O_3$ nanocomposite particles have not been examined before. Parts a and b of Figure 4 show that fairly uniform mesoporous silica layers were obtained over SiO_2/Fe_2O_3 nanoparticles with 25 nm thick solid SiO_2 shells. $MS/SiO_2/Fe_2O_3$ nanocomposite particles with irregular particle morphologies were produced with SiO_2/Fe_2O_3 nanoparticles with 4 nm thick solid SiO_2 shells (see Figure 4c). They were comprised of several SiO_2/Fe_2O_3 nanoparticles even at a low mesoporous silica coating level (i.e., when a low volume (100 μL) was used for the TEOS and C18TMS mixture).

The $MS/SiO_2/Fe_2O_3$ nanocomposite particles demonstrated type IV N_2 adsorption−desorption isotherms (Figure 5), confirming their mesoporosity. They all exhibited narrow BJH (Barret−Joyner−Halenda) pore size distributions with mesopores of <4 nm (Figure 5 inset). Reproducibly high BET (Brunauer−Emmett−Teller) surface areas were obtained for the $MS/SiO_2/Fe_2O_3$ nanocomposite particles (see Table 1). The particles with the thickest mesoporous silica shells (~21 nm thick) showed the highest BET surface area and mesoporosity. In comparison to the $MS/SiO_2/Fe_2O_3$ nanocomposite particles, the SiO_2/Fe_2O_3 nanoparticles with

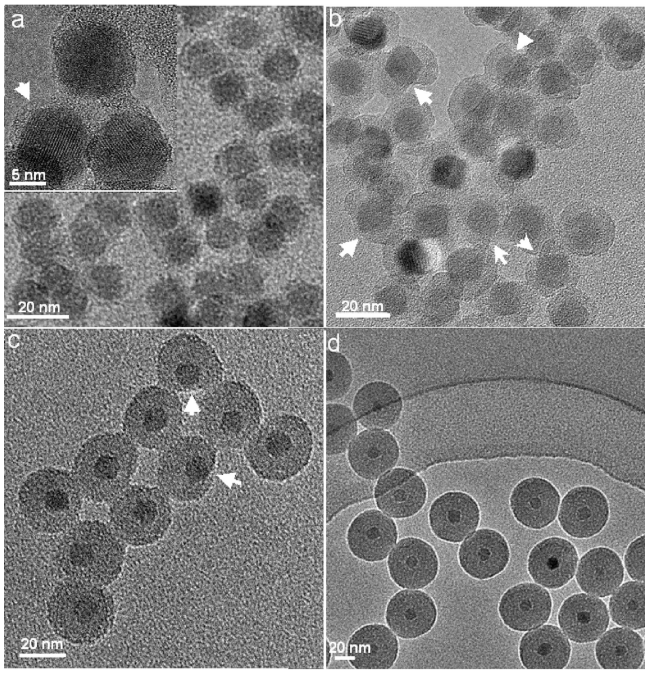

Figure 3. TEM micrographs of SiO_2/Fe_2O_3 nanoparticles with a SiO_2 shell thickness of (a) ~1.8 nm, (b) ~4 nm, (c) ~9 nm, and (d) ~25 nm.

(14) Büchel, G.; Unger, K. K.; Matsumoto, A.; Tsutsumi, K. *Adv. Mater.* **1998**, *10*, 1036.
(15) Kim, M.; Sohn, K.; Na, H. B.; Hyeon, T. *Nano Lett.* **2002**, *2*, 1383.
(16) Lu. A.-H.; Li, W. C.; Kiefer, A.; Schmidt, W.; Bill, E.; Fink, G.; Schüth, F. *J. Am. Chem. Soc.* **2004**, *126*, 8616.

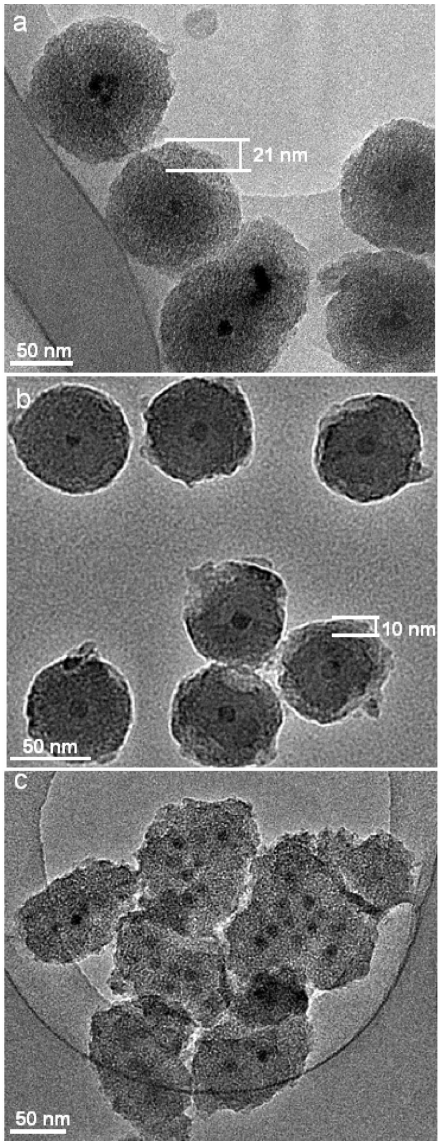

Figure 4. TEM micrographs of MS/SiO_2/Fe_2O_3 nanocomposite particles with (a) ~21 nm thick and (b) ~10 nm thick mesoporous silica layers and (c) irregular morphologies comprising several SiO_2/Fe_2O_3 nanoparticles. For the synthesis, (a) 260 μL, (b) 120 μL, and (c) 200 μL of a mixture of TEOS and C18TMS were used with SiO_2/Fe_2O_3 nanoparticles of (a,b) 25 nm thick and (c) 4 nm thick solid SiO_2 shells.

25 nm thick solid SiO_2 shells displayed a much smaller BET surface area and a lower porosity, which could be attributed to interparticle instead of intraparticle porosity.

Magnetic characterization was performed using a superconducting quantum interference device (SQUID). Field-dependent magnetization plots illustrated that bare Fe_2O_3 nanoparticles, SiO_2/Fe_2O_3 nanoparticles, and MS/SiO_2/Fe_2O_3 nanocomposite particles were hysteretic at 5 K (Figure 6). Raw data were presented in emu per g of sample. The bare Fe_2O_3 magnetic nanoparticles showed the highest magnetization value (saturation magnetization (M_s) ~57 emu/g) (Figure 6a). The M_s values of the SiO_2/Fe_2O_3 nanoparticles decreased with increasing shell thickness (40 emu/g and 3.6 emu/g for samples with shell thicknesses of 4 and 25 nm, respectively) (Figure 6, parts b and c). MS/SiO_2/Fe_2O_3 nanocomposite showed an even lower M_s value (1.5 emu/g) with the additional mesoporous silica layer (~21 nm thick). The reduction in M_s values could be attributed to the lower density of the

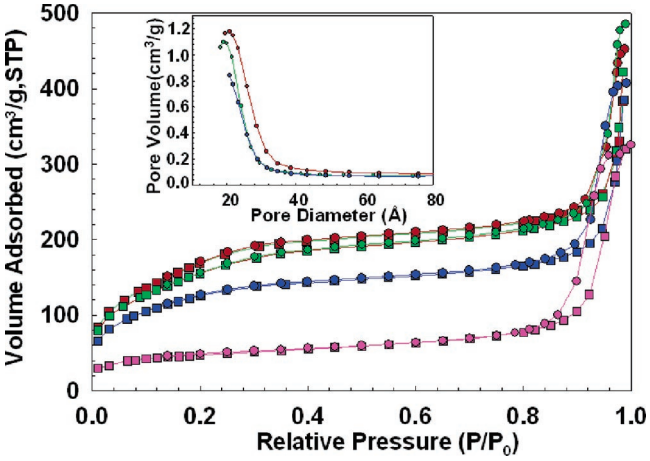

Figure 5. N_2 adsorption−desorption isotherms and pore size distributions (inset) of MS/SiO_2/Fe_2O_3 nanocomposite particles with ~21 nm thick (red) and ~10 nm thick (blue) mesoporous silica layers, and irregular morphologies (green), prepared according to the description in Figure 4a−c, respectively. N_2 adsorption−desorption isotherm (magenta) of SiO_2/Fe_2O_3 nanoparticles with 25 nm thick solid SiO_2 shells.

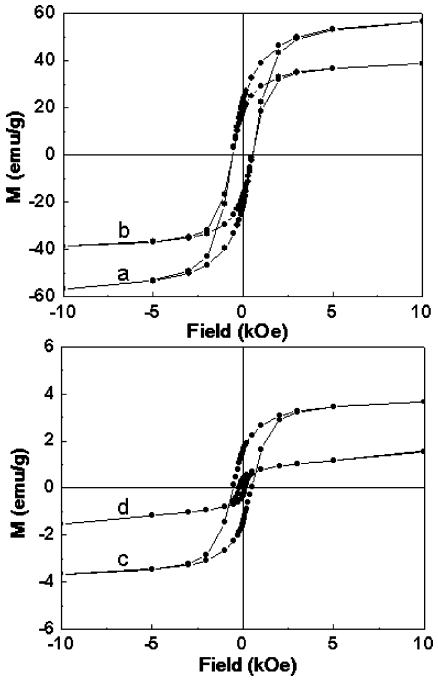

Figure 6. Field-dependent magnetization hysteresis loops of (a) bare Fe_2O_3 nanoparticles, (b) SiO_2/Fe_2O_3 nanoparticles with 4 nm thick SiO_2 shells, (c) SiO_2/Fe_2O_3 nanoparticles with 25 nm thick SiO_2 shells, and (d) MS/SiO_2/Fe_2O_3 nanocomposite particles with 25 nm thick SiO_2 shells and 21 nm thick mesoporous silica layer at 5 K.

Table 1. BET Surface Area and Total Pore Volume of the MS/SiO_2/Fe_2O_3 Nanocomposite Particles and SiO_2/Fe_2O_3 Nanoparticles Described in Figure 5

SiO_2 shell thickness in the SiO_2/Fe_2O_3 template (nm)	mesoporous silica layer thickness (nm)	BET surface area (m^2/g)	total pore vol (cm^3/g)
25	21	607	0.75
25	10	433	0.63
4	irregular	557	0.70
25	−	157	0.51

magnetic component in the SiO_2/Fe_2O_3 and MS/SiO_2/Fe_2O_3 samples. When their magnetization values were normalized to emu per gram of Fe_2O_3 content, comparable M_s values were obtained as those of the bare Fe_2O_3 nanoparticles (see SI).

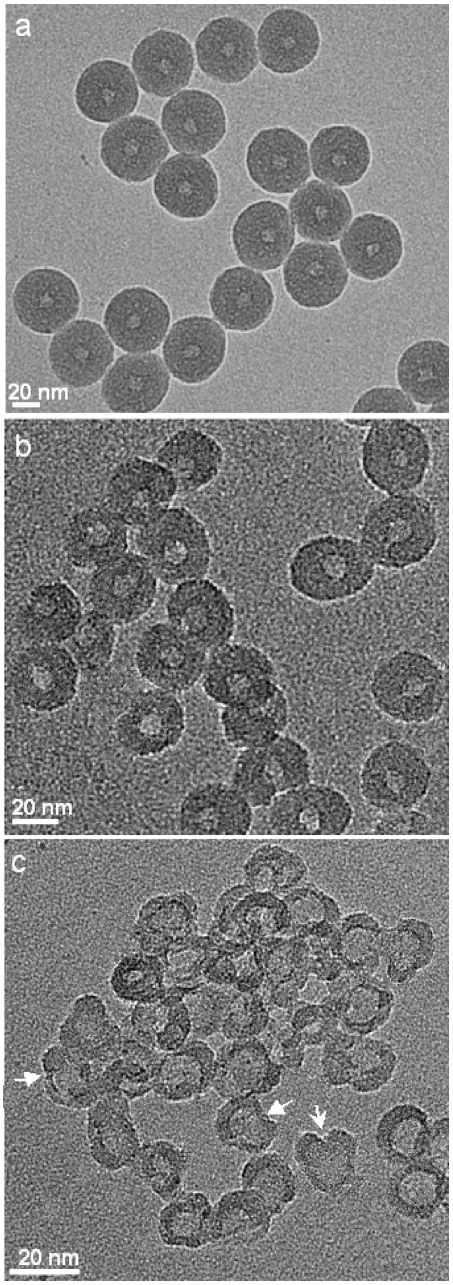

Figure 7. TEM micrographs of hollow SiO_2 balls, whose shell thickness was controlled by the SiO_2 coating thickness in the SiO_2/Fe_2O_3 nanoparticles to be (a) ~19 nm, (b) ~9 nm, and (c) ~4 nm.

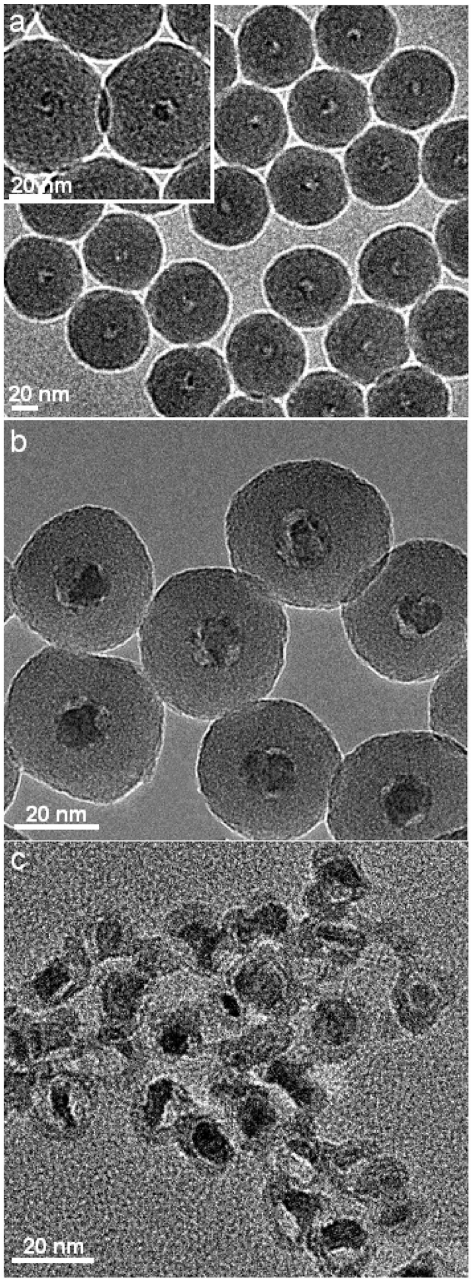

Figure 8. TEM micrographs of rattle-type SiO_2/Fe_2O_3 nanoballs. By varying the HCl concentration and etching time, Fe_2O_3 cores of (a) ~8 nm and (b) ~9 nm were obtained. (c) Fe_2O_3 cores of an irregular morphology were observed when SiO_2/Fe_2O_3 nanoparticles with thin SiO_2 shells of ~4 nm were used as the templates.

The bare Fe_2O_3 nanoparticles and the SiO_2/Fe_2O_3 nanoparticles with 4 nm SiO_2 coating exhibited similar coercivities, H_c ~530 Oe, at 5 K. The SiO_2/Fe_2O_3 nanoparticles with the thick 25 nm SiO_2 coating and the $MS/SiO_2/Fe_2O_3$ nanocomposite particles showed lower coercivities of 500 and 157 Oe, respectively. The significant decrease in coercivity in the latter could be attributed to changes in the SiO_2/Fe_2O_3 interfacial structure induced during annealing at 823 K for the porogen removal. This 7 h annealing process resulted in lowering the interfacial stresses and their contribution to the surface anisotropy of the magnetic core. X-ray diffraction (XRD) patterns showed that the Fe_2O_3 cores in the $MS/SiO_2/Fe_2O_3$ nanocomposite particles retained their crystallinity after calcination at 823 K (see the Supporting Information).

It was noted that all hysteresis loops in Figure 6 showed a remnant magnetization (M_r) to M_s ratio of 1/2. This value indicated that all four magnetic nanocomposite particles exhibited uniaxial magnetic anisotropy,[17] as expected for nanostructured γ-Fe_2O_3, which possessed weak magnetocrystalline anisotropies, leaving shape and surface effects to dominate their effective magnetic anisotropy densities.[18] This is in contrast, for example, to $CoFe_2O_4$ nanoparticles, which possess strong magnetocrystalline anisotropies. For the case of spherical particles, as observed herewith, surface effects and interfacial stresses[19] at the SiO_2/magnetic

(17) Stoner, E. C.; Wohlfarth, E. P. *Philos. Trans. R. Soc. London, Ser. A* **1948**, *240*, 599; reprinted in *IEEE Trans. Magn.* **1991**, *27*, 3475.
(18) Papaefthymiou, G. C. *Mater. Res. Soc. Symp. Proc.* **2001**, *635*, C.2.4.1.

core interface would be the dominant sources of magnetic anisotropy.

Our as-synthesized SiO_2/Fe_2O_3 nanoparticles could serve as a template to derive hollow nanoballs. Compared to conventional methods,[20−22] our synthesis produced more uniform and smaller hollow SiO_2 balls with tunable shell thickness. Size tunability in the range of <100 nm would be of importance in biomedical applications, such as in drug delivery systems[23] to control drug release rates and durations. Since our hollow SiO_2 balls were derived by etching away the Fe_2O_3 cores from the SiO_2/Fe_2O_3 nanoparticles using 20% HCl solution, they were structurally stable in the presence of water. Figure 7 demonstrates that hollow SiO_2 balls could be prepared with uniform shell thicknesses of 4−19 nm. Some of the hollow balls with thin SiO_2 shells were asymmetrical (noted by arrows in Figure 7c), reflecting the asymmetrically coated SiO_2 in the templating SiO_2/Fe_2O_3 nanoparticles (see Figure 3b). It should be noted that the Fe_2O_3 core for SiO_2/Fe_2O_3 nanoparticles used in this study was fixed at ∼12 nm; thus, the hollow core in the SiO_2 balls was set at ∼12 nm in diameter. The latter could be easily varied by controlling the size of the Fe_2O_3 nanocrystals used as the sacrificial core.[24]

With mild etching, it was possible to have partial removal of the Fe_2O_3 core in the SiO_2/Fe_2O_3 nanoparticles, producing rattle-type SiO_2/Fe_2O_3 nanoballs. Recent studies on rattle-type nanoballs have focused on polymer/metal[25−27] and SiO_2/metal[9b,15] systems. Rattle-type nanoballs with metal oxide cores would offer additional possibilities for the research and applications of nanocomposites. Our synthesis allowed the SiO_2 shell thickness of the rattle-type SiO_2/Fe_2O_3 nanoballs to be controlled by the SiO_2 coating thickness of the templating SiO_2/Fe_2O_3 nanoparticles. Furthermore, the Fe_2O_3 core size could be manipulated on the nanometer scale by varying the HCl concentration and etching time. For example, when SiO_2/Fe_2O_3 nanoparticles with ∼23 nm SiO_2 shells were etched by 20% HCl for 15 min, rattle-type SiO_2/Fe_2O_3 nanoballs with ∼8 nm Fe_2O_3 cores were produced (Figure 8a). When SiO_2/Fe_2O_3 nanoparticles with ∼11 nm SiO_2 shells were etched by 20% HCl for 2 min, rattle-type SiO_2/Fe_2O_3 nanoballs with ∼9 nm Fe_2O_3 cores were generated (Figure 8b). When SiO_2/Fe_2O_3 nanoparticles with ∼4 nm SiO_2 shells were etched by 10% HCl for 2 min, rattle-type SiO_2/Fe_2O_3 nanoballs with irregular Fe_2O_3 morphology were obtained (Figure 8c). The rattle-type SiO_2/Fe_2O_3 nanoballs could be easily collected by a magnet, indicating that the magnetic property of the Fe_2O_3 cores was preserved after the mild etching.

In conclusion, uniform SiO_2/Fe_2O_3 nanoparticles have been fabricated with well-controlled shell thickness. These nanoparticles were successfully used as templates for the synthesis of mesoporous silica-coated SiO_2/Fe_2O_3 nanoparticles, rattle-type SiO_2/Fe_2O_3 nanoballs, and hollow SiO_2 nanoballs.

Acknowledgment. The authors thank Dr. S. T. Selvan (Institute of Bioengineering and Nanotechnology (IBN)) for helpful discussions and Dr. G. Hadjipanayis and Dr. Y. Huang for facilitating the acquisition of SQUID data at the University of Delaware. This work was supported by IBN (Agency for Science, Technology and Research, Singapore).

Supporting Information Available: Cytotoxicity of SiO_2/Fe_2O_3 nanoparticles, normalized field-dependent magnetization of SiO_2/Fe_2O_3 nanoparticles at 5 K, and XRD patterns of SiO_2/Fe_2O_3 nanoparticles and $MS/SiO_2/Fe_2O_3$ nanoparticles. This material is available free of charge via the Internet at http://pubs.acs.org.

CM0512979

(19) (a) O'Handley, R. C. *Modern Magnetic Materials*; John Wiley & Sons: New York, 2002. (b) Yu, J.-H.; Lee, C.-W.; Im, S.-S.; Lee, J.-S. *Adv. Mater. Sci.* **2003**, *4*, 55.
(20) Lu, Y.; McLellan, J.; Xia, Y. *Langmuir* **2004**, *20*, 3464.
(21) Fujiwara, M.; Shiokawa, K.; Tanaka, Y.; Nakahara, Y. *Chem. Mater.* **2004**, *16*, 5420.
(22) Caruso, F. *Top. Curr. Chem.* **2003**, *227*, 145.
(23) (a) Barbe, C.; Bartlett, J.; Kong, L.; Finnie, K.; Lin, H. Q.; Larkin, M.; Calleja, S.; Bush, A.; Calleja, G. *Adv. Mater.* **2004**, *16*, 1959. (b) Roy, I.; Ohulchanskyy, T. Y.; Pudavar, H. E.; Bergey, E. J.; Oseroff, A. R.; Morgan, J.; Dougherty, T. J.; Prasad, P. N. *J. Am. Chem. Soc.* **2003**, *125*, 7860.
(24) (a) Rockenberger, J.; Scher, E. C.; Alivisatos, A. P. *J. Am. Chem. Soc.* **1999**, *121*, 11595. (b) Shen, S.; Zeng, H. *J. Am. Chem. Soc.* **2002**, *124*, 8204.
(25) Crooks, R. M.; Zhao, M.; Sun, L.; Chechik, V.; Yeung, L. K. *Acc. Chem. Res.* **2001**, *34*, 181.
(26) Antipov, A. A.; Sukhorukov, G. B.; Fedutik, Y. A.; Hartmann, J.; Giersig, M.; Möhwald, H. *Langmuir* **2002**, *18*, 6687.
(27) Kamata, K.; Lu, Y.; Xia, Y. *J. Am. Chem. Soc.* **2003**, *125*, 2384.